Comparison of full-scale PIV measurements with CFD simulations of a ship propeller inflow

Miloš Birvalski[1,*], Serge L. Toxopeus[2], Gijs D. Struijk[1], Dmitriy Ponkratov[3]
1: Performance at Sea dept., MARIN, The Netherlands
2: Research & Development dept., MARIN, The Netherlands
3: JoRes Project, United Kingdom
* Corresponding author: m.birvalski@marin.nl

1. Introduction

Flow around the ship's hull and specifically the inflow conditions of the propeller(s) critically influence the propeller efficiency and cavitation behaviour. In a typical single-propeller vessel, the hull of the ship creates a velocity deficit in the top part of the propeller disk. In this relatively limited region, the velocity vectors have a different angle of attack with the blade leading edge than what the propeller was designed for. This creates suitable conditions for cavitation, which is the main source of noise and vibration both inside the vessel as well as in the marine environment. In order to accurately predict this critical part of the flow, CFD simulations have a requirement for validation data. Recently, full-scale measurements of the flow around a ship were performed by [1], [2], [3] and [4]. Such data was also recently acquired within the JoRes joint industry project (JIP), where the current authors applied a novel full-scale stereo-PIV device (called 'FlowPike') onboard a large sailing vessel. Initial results were presented in Birvalski et al. [5]. The current study uses the same data, focusing on two new aspects: 1) quantifying the uncertainty of the PIV measurements by using both the measurements performed at MARIN and at sea, 2) presenting first comparisons between the PIV results and CFD simulations of the full-scale flow.

2. Measurement device

The FlowPike is a stereo-PIV system (2D3C) built into a steel housing that can be fixed to the outside of the vessel (see Figure 1). The housing (diameter 0.45 m, length ~2.5 m) contains two cameras (PCO.edge 5.5 MPx, sCMOS 2560x2160 px^2, 16-bit, 6.5 μm pixel size) with Canon EF 50 mm/$f^{\#}$1.4 lenses coupled to the camera with Scheimpflug mounts. The housing also contains a laser head (Lumibird EverGreen HP 532 nm, 340 mJ/pulse, 20 Hz max. repetition rate). The rest

of the power, cooling and data collection equipment is placed inside the vessel, connected to the housing using 10 m long cables and hoses. For connecting the FlowPike to the inside of the ship, one hull penetration is necessary. During current measurements, the FlowPike was running at 10 Hz, while the laser was used at full power.

The FlowPike stereo-PIV configuration is symmetric, i.e. the laser sheet was positioned in the middle between the two cameras. The cameras are placed 1.75 m apart and their views form a 40° angle with respect to each other; they focus on a point 2.5 m away from the centre of the device. The field of view (FOV) in which measurements are performed is ~650 mm wide, ~1400 mm long, beginning 2 m away from the FlowPike. Since the device can rotate in the plane of the FOV (i.e. in the plane of the laser sheet), the width of the FOV can also be expressed as an angle; this is approximately 10°. Further, the FlowPike can rotate in a span of approximately 170° from side to side, although in the current measurements the total span was 140°.

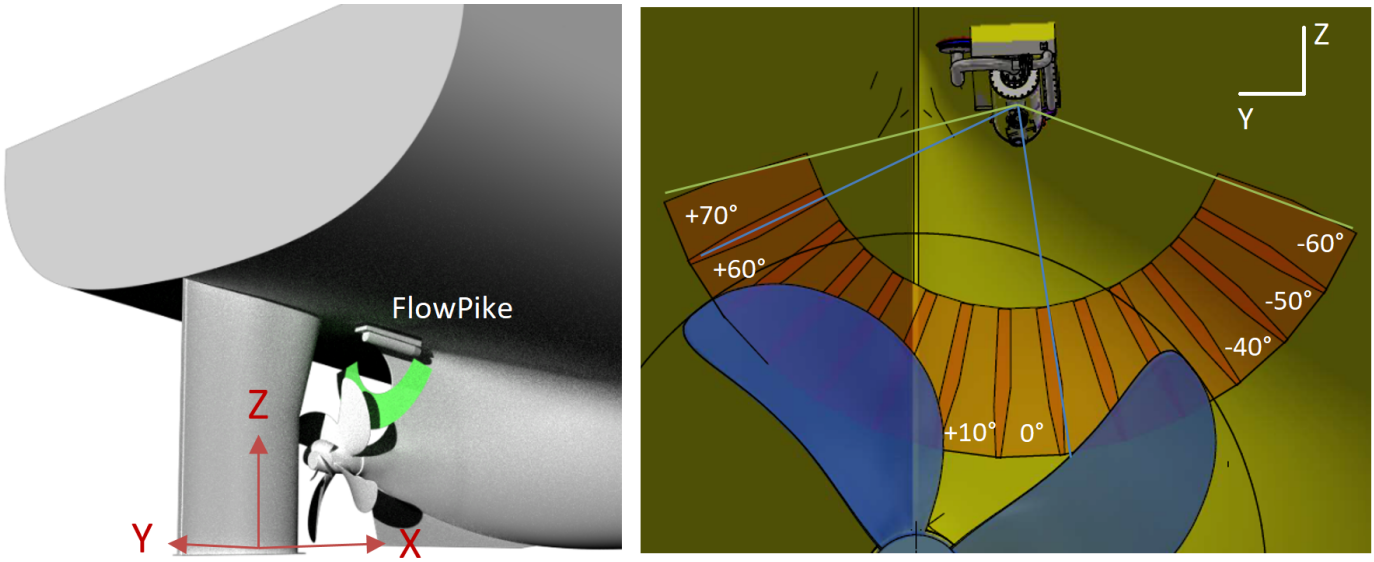

Figure 1 Position of the FlowPike on the ship with the coordinate system at station zero, centreline and baseline (left). Aft view of the FlowPike fixed to the hull above the propeller (right). The two blue lines show the 70° span and the two green lines show a 140° span of the two types of measurements that were performed (see Table 1). Individual measurement areas are also shown along with the angular position of the centreline of each area.

During the commissioning of the FlowPike, the system was calibrated and tested in MARIN's Deepwater Tank (DT). The calibration was performed using a 1x1 m^2 white board (two-sided, single level) onto which a grid of black dots was printed (the dots were 37.5 mm in diameter with a dot-to-dot distance of 75 mm). Approximately ten image pairs were acquired in varying orientations of the calibration board (with the first image pair aligned with the laser sheet), as required by the calibration algorithm of DaVis. Before deploying on a trial, the PIV system was calibrated again. The calibrated FlowPike was then shipped to the trial location and no further calibration on site was necessary.

3. Measurement campaigns

Two measurement campaigns were performed with the FlowPike device. The first was a test campaign in MARIN's Deepwater Tank which consisted of performing runs down the basin at constant speed. The goal was to verify the full operability of the newly-built FlowPike as well as to quantify its accuracy in a uniform flow field. The carriage speed was varied between 0.5 m/s and 4.0 m/s. At each speed, between 200 and 300 image pairs were recorded. This was considered sufficient because the water was still and the carriage was moving at a constant speed.
The second measurement campaign was performed at sea. During the JoRes project sea trial, full-scale PIV measurements were done onboard a 50,000 deadweight ton tanker sailing in the Persian Gulf. The goal of the trial was to gather detailed data on propeller inflow and the speed/power characteristics of the ship. Besides the PIV data, environmental conditions were recorded and various ship parameters relevant for its speed/power performance were measured.

Table 1 Overview of full-scale PIV measurements performed during the sea trials of the JoRes project. Multiple measurements make up a single run. Subsequent runs form pairs, e.g. run 3 is in one direction, while run 4 is in the opposite direction along the same track.

Measurements	Run	Propeller rotation rate [min^{-1}]	Ship velocity [m/s]	FlowPike angles [°]	Images per measurement
1-7	3	75	5.79	60; 50; 40; 30; 20; 10; 0	800
8-14	3	75	5.79	60; 50; 40; 30; 20; 10; 0	800
15-20	3	75	5.79	55; 45; 35; 25; 15; 5	800
21-27	4	75	5.79	60; 50; 40; 30; 20; 10; 0	800
28-34	4	75	5.79	60; 50; 40; 30; 20; 10; 0	800
35-40	4	75	5.79	55; 45; 35; 25; 15; 5	800
41-47	5	75	5.79	70; 50; 30; 10; -10; -30; -50	1200
48-54	5	75	5.79	60; 40; 20; 0; -20; -40; -60	1200
55-61	6	75	5.79	70; 50; 30; 10; -10; -30; -50	1200
62-68	6	75	5.79	60; 40; 20; 0; -20; -40; -60	1200
69-75	7	90	6.86	60; 50; 40; 30; 20; 10; 0	800
76-82	7	90	6.86	60; 50; 40; 30; 20; 10; 0	800
83-88	7	90	6.86	55; 45; 35; 25; 15; 5	800

89-95	8	90	6.86	60; 50; 40; 30; 20; 10; 0	800
96-102	8	90	6.86	60; 50; 40; 30; 20; 10; 0	800
103-108	8	90	6.86	55; 45; 35; 25; 15; 5	800
109-115	9	90	6.86	70; 50; 30; 10; -10; -30; -50	1200
116-122	9	90	6.86	60; 40; 20; 0; -20; -40; -60	1200
123-129	10	90	6.86	70; 50; 30; 10; -10; -30; -50	1200
130-136	10	90	6.86	60; 40; 20; 0; -20; -40; -60	1200

As usual with speed/power trials, the measurements were performed as straight reciprocal runs. The runs were done at two propeller rotation rates (RPM): 75 min^{-1} and 90 min^{-1}. At each RPM, two double (reciprocal) runs were done. During the first pair of runs (run 3 and 4, see Table 1), the FlowPike was sweeping an area 70° wide, from +65° to -5° with a step size of 5°, with positive oriented towards port and zero defined as the position in which the FlowPike is at the middle point between its extreme extents in terms of rotation. During the second pair of runs, done at the same RPM, a 140° wide area was swept, from +75° to -65° with a step size of 10°. By 'sweeping' it is meant that the FlowPike measured 800 or 1200 image pairs (i.e. 80 or 120 seconds) at a certain angle after which the measurement was stopped, the FlowPike rotated to the next angular position and a new measurement started. The exact order of measurements is shown in Table 1. It can be seen that the sweep from one extreme angle to the other was not done in one pass, but in several passes. Some angular positions were measured twice during the same run (e.g. measurements 1-7 are at the same angles as 8-14), while subsequent passes focused on achieving the flow fields to overlap (measurements 15-20). This strategy ensured that there would be no gaps between the velocity fields and added an additional level of time-separation (independence) to the samples measured at each point in the flow.

4. PIV uncertainty quantification

In order to compare CFD and PIV, it is important to quantify the uncertainty of PIV measurements. In the current study, the total uncertainty is assumed to have two components: systematic (bias) and non-systematic (random). The bias uncertainty was estimated from the measurements in the DT, while the random uncertainty was estimated from the full-scale trials.

The measurement campaign in the DT consisted of making runs down the tank at a constant and accurately know speed; the uncertainty of the tank carriage speed is ≤0.06%, which is much lower than the expected uncertainty of PIV measurements. The carriage speed was, therefore, considered

exact and the possible secondary (residual) currents in the basin were neglected. The FlowPike was fixed to the carriage such that it was aligned with the movement direction. The FlowPike FOV was pointing vertically downwards, with the laser sheet perpendicular to the flow direction. Therefore, the velocity perceived by the PIV system consisted of only one component passing through the measurement plane whose magnitude was equal to the carriage speed. Before measuring, the FlowPike was calibrated (RMS of the reprojection error was 1 pixel) and the flow was seeded with 50-60 μm diameter plastic spheres.

The instantaneous velocity fields resulting from PIV processing were averaged to arrive at mean velocity fields. Since the basin water was assumed to be completely still and the carriage was traveling at a known constant speed, every deviation of the vectors from the carriage speed is a measure of velocity error (see Figure 2). The mean velocity fields reveal a systematic deviation from the expected uniform field that corresponds to patterns generated by peak locking. Specifically, the peak locking phenomenon results in flow fields that show 'waves' of velocity magnitude along the length of the field of view (i.e. in the depth direction of the tank). At places where the flow velocity corresponds to integer values of pixel displacement the velocity is accurate, while at places where the pixel displacement is between the integer values the velocity shows an error.

The presence of peak locking can also be inferred theoretically by calculating the ratio of the particle image diameter to the pixel size. The particle image diameter can be estimated using:

$$d_\tau = \sqrt{\left(M_0 d_p\right)^2 + d_s^2 + d_a^2}$$

Here, $M_0 = 0.009\text{-}0.026$ is the magnification of the current system, $d_p = 60$ μm is the seeding particle diameter, d_s is the diffraction-limited component of the particle image diameter (calculated below) and d_a is the component of the image diameter originating from lens imperfections (this component is neglected). Taking the best case scenario where $M_0 = 0.026$,

$$d_s = 2.44(1 + M_0)f^{\#}\lambda = 2.44 \cdot (1 + 0.026) \cdot 2.5 \cdot 532\ \text{nm} = 3.33\ \mu\text{m}$$

In this equation, $f^{\#} = 2.5$ is the aperture stop used in the measurements (both in the basin and during the trial) and $\lambda = 532$ nm is the wavelength of the laser. The total image diameter was $d_\tau = 3.68$ μm which is much smaller than 6.5 μm (camera pixel size), resulting in peak locking.

During the trial, the same magnification and the same aperture size were used. The natural seeding particles present at sea were likely also of approximately the same size (see [5]) as the artificial

seeding used in the basin. This means that peak locking affects the trial results in a similar way as it does the basin results.

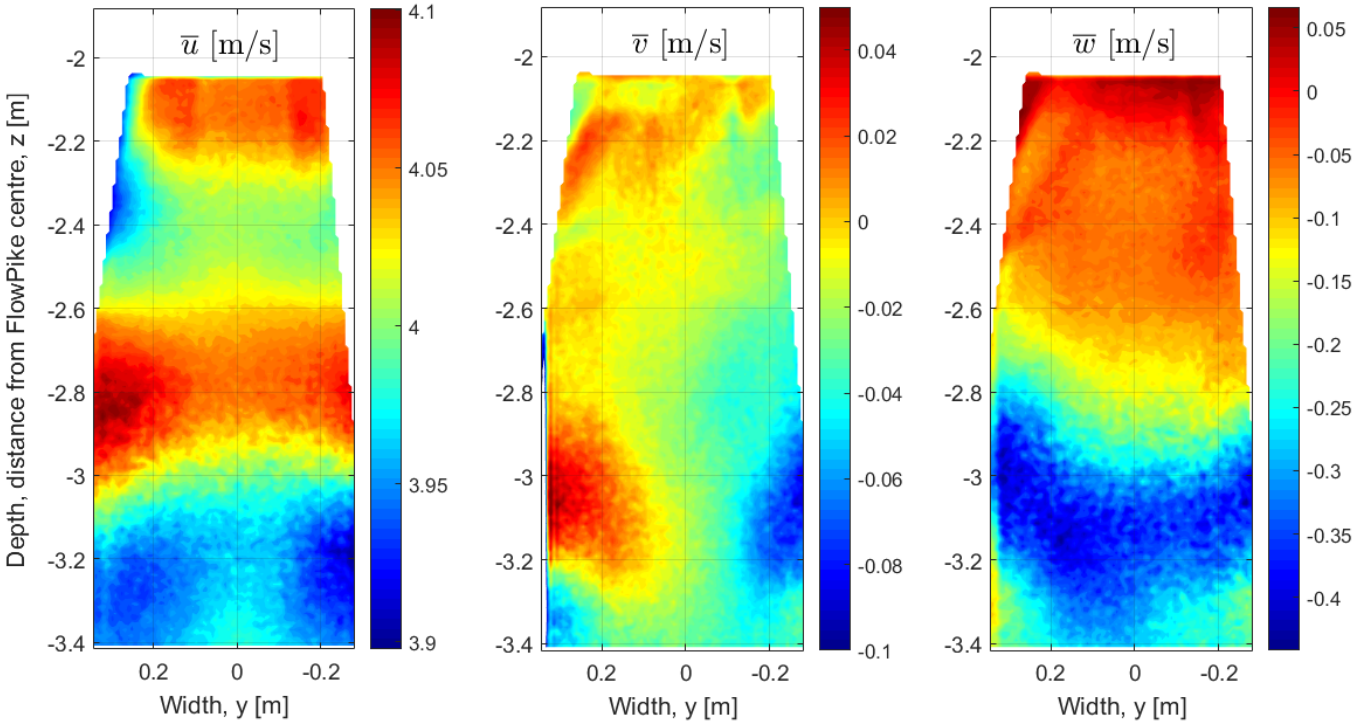

Figure 2 Averaged flow fields measured in uniform flow (4.00 m/s in the direction of the x-axis) in the Deepwater Tank of MARIN. The coordinate system is positioned in the centre of the FlowPike.

In terms of uncertainty quantification, the peak locking introduces a bias into the velocity field results. The bias was quantified by calculating the standard deviation of the error (the difference between the measured and the known flow velocity) using all the instantaneous vectors from one measurement. This was done for measurements at 1 m/s, 2 m/s, 2.5 m/s, 3.6 m/s and 4 m/s. Then, the standard deviation was scaled with the magnitude of velocity for each case. The resulting uncertainty is similar for different measurements:

Table 2 Bias uncertainty [%] of the PIV measurements for different carriage velocities expressed as percentage of the total velocity magnitude. (u, v, w) are velocity components corresponding to the (x, y, z) axes that are oriented the same as in the ship's coordinate system (i.e. x-axis is in the direction of the flow).

Velocity component	Carriage speed					Average bias uncertainty, $U_{bias,x}$, $U_{bias,y}$, $U_{bias,z}$ [%]
	1.0 [m/s]	2.0 [m/s]	2.5 [m/s]	3.6 [m/s]	4.0 [m/s]	
u	2.9	2.5	2.5	2.0	1.9	2.4
v	1.9	1.6	1.6	1.6	1.6	1.7
w	8.6	7.8	7.9	7.4	7.3	7.8

As shown, the main velocity component in the out-of-plane direction has a bias uncertainty of 2.4% on average, while the maximum uncertainty is in the direction of the apparent movement of the seeding particles in the images that amounts to 7.8%.

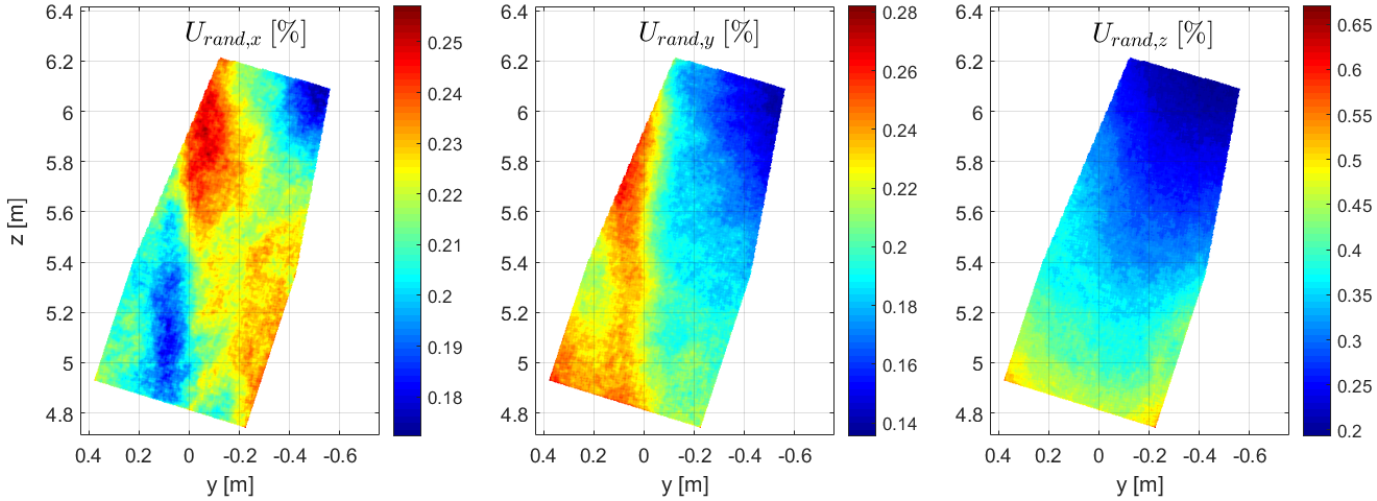

Figure 3 Random uncertainty of the three velocity components in measurement 118 (90 min^{-1}, +20°). The result is expressed in percentage, scaled with the local velocity magnitude.

The random component of uncertainty was assessed using data from the JoRes sea trials. Since in these measurements the true value of velocity was unknown, the uncertainty was calculated as the standard deviation of the mean velocity. This value was obtained in several steps. First, a few representative FlowPike angles were selected where the uncertainty will be assessed. These were the extreme angles of rotation (+70° and -60°) as well as the angle that was centred on the wake peak (+20°); the wake peak is the part of the flow at the centreline of the vessel where the velocity deficit and flow unsteadiness is the highest. Besides this, a few angles in between the wake peak and the extremes were chosen. For all these positions and for different runs, the random uncertainty was calculated in each vector position. This resulted in uncertainty maps; an average value of uncertainty was calculated for each map (see Figure 3). It was noticed that the highest value of random uncertainty was consistently obtained in measurements performed in the wake peak. These were approx. 2-3 times higher than at extreme angles which measured in a more steady part of the flow. As a measure of the overall random uncertainty level, the values at the wake peak were chosen (averaged across different measurements performed at +20°):

Table 3 Random uncertainty [%] of the PIV measurements in the JoRes trial expressed as percentage of the total velocity magnitude. (u, v, w) are velocity components corresponding to the (x, y, z) axes that are oriented the same as in the ship's coordinate system (i.e. x-axis is in the direction of the flow).

Velocity component	Average random uncertainty, $U_{rand,x}$, $U_{rand,y}$, $U_{rand,z}$ [%]

u	0.2
v	0.2
w	0.3

Compared to the bias uncertainty, these values are small. This is due to the relatively large number of image pairs that were collected for each case; almost every position in the flow within each run was sampled 2400 times (3x800 or 2x1200). Nevertheless, random uncertainty forms a part of total uncertainty so it should be added to the bias uncertainty by linearly adding the two variances:

$$U_{tot,i} = \sqrt{U_{bias,i}^2 + U_{rand,i}^2}, \quad \text{where } i = x, y, z$$

When plotting, the total standard deviation is doubled to present a confidence interval at the 95% level ($\pm 2U_{tot}$). This is done separately for each velocity component. Overall, the uncertainty is considered sufficiently small for the purpose of comparison to CFD calculations. In future applications of the FlowPike, however, measures against peak locking (diffraction filters, defocusing, reducing the aperture opening, etc.) can be applied in order to reduce the contribution of the bias uncertainty component.

5. CFD calculations

For the runs at 6.86 m/s (90 min^{-1}), preliminary CFD calculations were performed to estimate the ship propulsion performance and to generate flow field data for comparison to the PIV results.
As the calculations were performed within a wider joint industry project that had the aim of benchmarking CFD calculations of various parties against a common PIV dataset, the solution domain size and boundary conditions were selected based on instructions provided within JoRes. With the origin at the aft perpendicular (station zero), centreline and baseline, the inlet was located at x=535.5 m (2.92L_{pp}), the outlet at x=-535.5 m (-3L_{pp}), the port side and starboard boundaries at y=±357 m (±2L_{pp}), the top at z=89.25 m (0.5L_{pp}) and the bottom at z=-267.75 m (-1.5L_{pp}). At the inlet, an inflow Dirichlet boundary condition for the velocity was applied. At all other exterior boundaries a constant pressure Dirichlet condition was used. At the hull surfaces, no-slip conditions were applied.
The geometry consisted of: hull, rudder, centre skeg and FlowPike. The propeller geometry was not taken into account (see below) and was replaced by a dummy shaft. A grid was generated using Hexpress using a procedure similar to that of Crepier [6], with refinement zones applied to

capture gradients in the flow. Additionally, refinements were applied to capture the free surface deformation. Since the centre skeg and the presence of the FlowPike make the geometry asymmetric, both port and starboard side of the geometry are modelled. The height of the first cell on the hull surface was set to 5 mm ($2.8 \cdot 10^{-8} L_{pp}$), to resolve the gradients in the boundary layer. This avoids the use of wall functions. The resulting grid consists of 52 million cells and has 903,000 cells on the ship surface. An impression of the grid is shown in Figure 4.

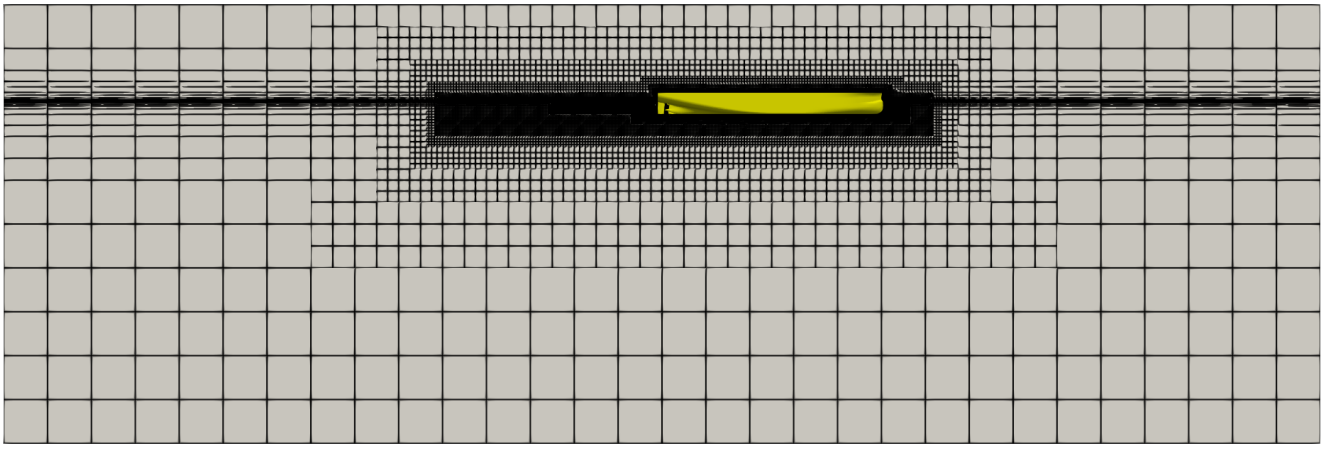

Figure 4: Impression of the grid around the JoRes tanker.

The computations were performed using the MARIN in-house solver ReFRESCO v2023.1 [7], which is a CFD solver based on a finite volume discretization of the continuity and momentum equations written in strong conservation form. The solver uses a fully collocated arrangement and a face-based approach that enables the use of cells with an arbitrary number of faces. Picard linearization is applied and segregated or coupled approaches are available with mass conservation ensured using a SIMPLE-like algorithm [8] and a pressure-weighted interpolation technique to avoid spurious oscillations [9]. Thorough code verification is performed for all releases of ReFRESCO [10].

For the present calculations, a volume-of-fluid technique is used to capture the free surface [11] and the two-equation k-ω SST turbulence model by Menter [12] is used to solve the turbulent flow. To simplify the computations, the propeller was modelled using body forces by coupling ReFRESCO with the boundary element code PROCAL (RANS-BEM coupling). In PROCAL, the potential flow around the propeller is computed based on inflow computed by ReFRESCO. More information can be found in Rijpkema et al. [13]. The PBCF has not been modelled in the computation, which may lead to a small mismatch in the predicted performance of the propulsion system.

During the calculation, the ship was free to trim and sink using grid deformation, and captive in all other degrees of freedom. To achieve self-propulsion, the propeller rotation rate was adjusted to arrive at an overall zero longitudinal force.
According to the JoRes JIP instructions, roughness was to be included in the CFD computation, while the bilge keels and superstructure resistance were neglected, but added as an additional resistance force in the self-propulsion evaluation. The roughness model used was based on Nikuradse correlations [14] and used specified equivalent sand grain roughnesses depending on the different surfaces. More details can be found in Eça et al. [15].

6. Results comparison

When running at self-propulsion at 6.86 m/s, a total resistance on the modelled hull surface of 511 kN was predicted. Together with the estimated resistance of the bilge keels and superstructure of 25 kN, this amounts to an overall resistance and therefore also propulsor thrust of 536 kN. Comparing with the sea trial results, an RPM was found which is 3.2% lower than the trial value, a torque Q_p of the same value as during the trials and subsequently a delivered power P_d of about 3.6% below the trial results. Considering the simplification of the propeller by using the RANS-BEM coupling, neglecting of the propeller boss cap fins (PBCF) and the absence of the bilge keels and superstructure in the computations, this is considered to be a very promising outcome.

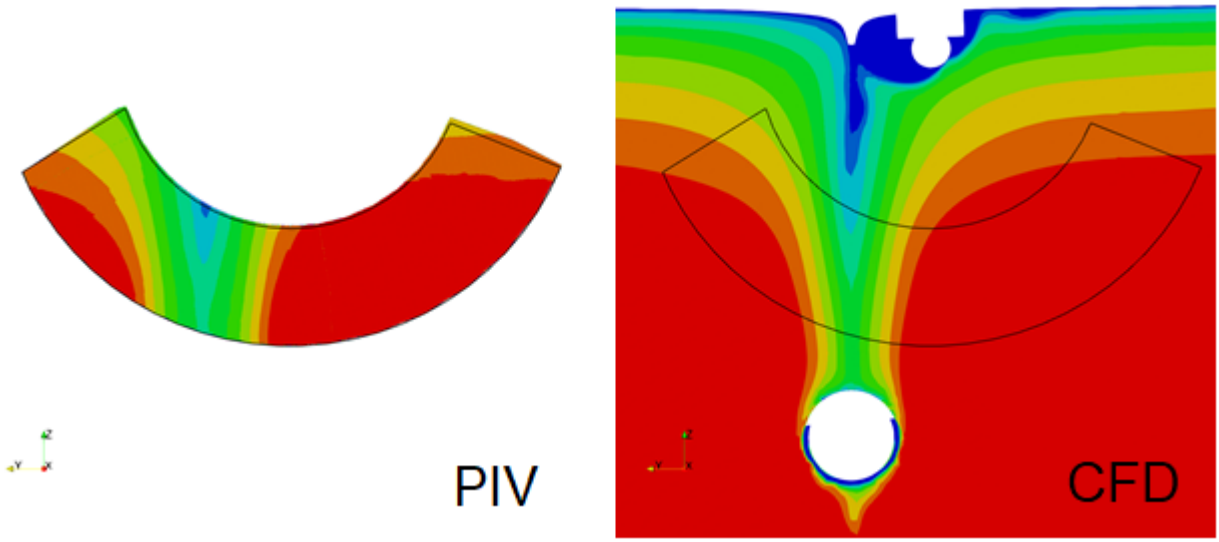

Figure 5 Comparison of velocity magnitude between PIV and CFD. Both results are shown using the same velocity scale. The scale itself is not shown since the results are currently a part of a blind CFD benchmarking study.

The flow field at the location of the PIV measurements has also been computed and compared to the trial results, see Figure 5. Qualitatively, it is seen that the wake peak coming from the centreline

towards the propeller is captured well, as is the boundary layer coming from the hull. However, quantitatively, the PIV result seems to predict a somewhat deeper wake peak than the CFD. Besides this, the boundary layer seems to be slightly thicker in the trials, as seen in the top right corner of the PIV measurement area. On average, the comparison errors between the CFD and the trials are about 5%, with a standard deviation of less than 6%. The largest errors occur in the wake peak and close to the hull surface (top of the measurement area).

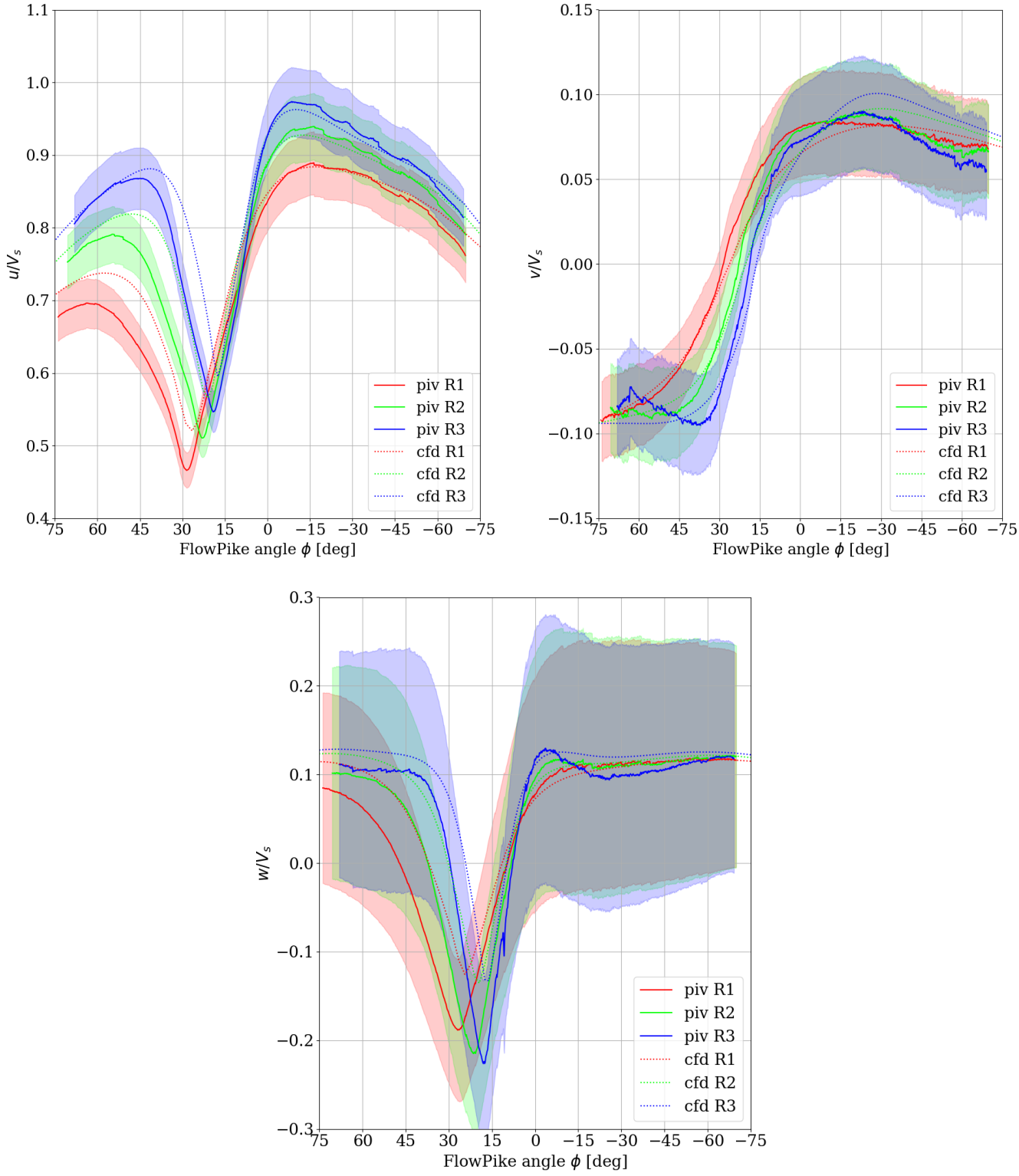

Figure 6 Comparison of velocity between PIV and CFD, for three radial distances from the FlowPike (R1 < R2 < R3). The velocity was scaled with V_s=6.86 m/s. The uncertainty is shown with 95% confidence bounds (±2U_{tot}).

Figure 6 presents the comparison of velocity components obtained with PIV and from CFD for three radial distances from the FlowPike. The PIV results are plotted including their estimated uncertainty band (±2U_{tot}, shaded area). R1 is a radial distance close to the inner circle of the PIV

measurement plane, and R3 is close to the outer circle. R2 lies in the middle of the measurement plane. Since the PIV data is currently a part of a CFD benchmarking study, the exact positions of R1, R2 and R3 are not revealed to prevent influencing the outcome of the study.
It can be seen that on the starboard side of the PIV plane (negative angles), the CFD results of the three components fall almost completely within the PIV bands, which means that no significant differences exist between the CFD and PIV in that area. On port side (positive angles), an overprediction of the axial and vertical (u and w) velocities is seen. Further study is required to explain the differences, but it may be that the roughness influence in CFD is underestimated, resulting in a too thin boundary layer.

7. Conclusions

- Recently, two measurement campaigns were performed using a novel full-scale stereo-PIV device built to measure flows around vessels sailing at sea. During the first campaign, performed in one of MARIN's basins, the device was commissioned. The second campaign was performed during a sea trial; it resulted in propeller inflow data that can be used for validating CFD codes.
- The uncertainty of the PIV measurements was assessed using both campaigns. In the basin, uncertainty bias could be determined by comparing the PIV results with the carriage speed. At sea, the random part of uncertainty was determined by quantifying the standard deviation of the mean velocity for all three velocity components in the wake peak area of the propeller inflow. Overall, the uncertainty was found to be acceptably small, given the scale of the measurement and the necessity to work with naturally occurring seeding particles in the sea.
- CFD calculations of the same full-scale flow were performed using an in-house flow solver. The CFD results predicted the propeller RPM and the delivered power measured during the full-scale trial well, which gives confidence in the ability of CFD to predict ship trial performance. The comparison of the flow fields was good, with the PIV results demonstrating that full-scale PIV can be done reliably, and that the CFD is able to capture the major features of the flow in the considered area. For a large part of the flow field, the CFD was within the measurement uncertainty band. The wake peak was slightly underpredicted, which may be related to roughness effects on the boundary layer thickness.
- Further study is required to determine whether modelling the actual propulsion will improve the comparison with the trials. Additionally, grid sensitivity studies are needed to

estimate the numerical uncertainty in the results and to obtain a validation uncertainty for the different propulsion variables. This will enable further validation of the computation.

8. Acknowledgements

The support of JoRes project partners and the vessel owner is gratefully acknowledged. Martijn Elbertsen (MARIN) and Just Settels (MARIN) are acknowledged for their help in preparing and executing the trial. This research was partly funded by the Dutch Ministry of Economic Affairs.

9. References

[1] A. Kleinwächter, E. Ebert, R. Kostbade, K. Hellwig-Rieck, H. Heinke and N. Damaschke, "Full-scale total wake field PIV-measurements for an enhanced cavitation prediction," in *17th Symposium on Applications of Laser Technologies to Fluid Dynamics*, Lisbon, Portugal, 2014.

[2] A. Kleinwächter, E. Ebert, R. Kostbade, K. Hellwig-Rieck, H. Heinke and N. Damaschke, "PIV as a novel full-scale measurement technique in cavitation research," in *3rd International Symposium on Marine Propulsors*, Austin, USA, 2015.

[3] Y. Inukai, Y. Sudo, H. Osaki, T. Yanagida, M. Mushiake and S. Kawanami, "Extensive full-scale measurement on propeller performance of 14000 TEU container ship," in *3rd Hull Performance & Insight Conference* , UK, 2018.

[4] N. Sakamoto, H. Kobayashi and K. Ohashi, "Estimation of flows around a full-scale ship by structured overset RANS code 'NAGISA'," in *11th International Workshop on Ship and Marine Hydrodynamics*, Hamburg, Germany, 2019.

[5] M. Birvalski, G. D. Struijk and D. Ponkratov, "Full-scale PIV measurements of the propeller inflow," in *15th International Symposium on Particle Image Velocimetry - ISPIV*, San Diego, US, 2023.

[6] P. Crepier, "Ship Resistance Prediction: Verification and Validation Exercise on Unstructured Grids," in *VII International Conference on Computational Methods in Marine Engineering (MARINE)*, Nantes, France, 2017.

[7] G. Vaz, F. A. P. Jaouen and M. Hoekstra, "Free-Surface Viscous Flow Computations. Validation of URANS Code FreSCo," in *28th International Conference on Ocean, Offshore and Arctic Engineering (OMAE)*, Honolulu, USA, 2009.

[8] C. M. Klaij and C. Vuik, "SIMPLE-Type Preconditioners for Cell-Centered, Colocated Finite Volume Discretization of Incompressible Reynolds-Averaged Navier-Stokes Equations," *International Journal of Numerical Methods in Fluids* , vol. 71, no. 7, pp. 830-849, 2013.

[9] T. F. Miller and F. W. Schmidt, "Use of a Pressure-Weighted Interpolation Method for the Solution of the Incompressible Navier-Stokes Equations on a Nonstaggered Grid System," *Numerical Heat Transfer,* vol. 14, no. 2, pp. 213-233, 1988.

[10] L. Eça, C. M. Klaij, G. Vaz, M. Hoekstra and F. S. Pereira, "On Code Verification of RANS Solvers," *Journal of Computational Physics,* vol. 310, pp. 418-439, 2016.

[11] C. M. Klaij, M. Hoekstra and G. Vaz, "Design, Analysis and Verification of a Volume-Of-Fluid Model with Interface-Capturing Scheme," *Computers & Fluids* , vol. 170, pp. 324-340, 2018.

[12] F. R. Menter, M. Kuntz and R. Langtry, "Ten Years of Industrial Experience with the SST Turbulence Model," in *4th International Symposium on Turbulence, Heat and Mass Transfer* , Antalya, Turkey, 2003.

[13] D. R. Rijpkema, A. R. Starke and J. Bosschers, "Numerical Simulation of Propeller-Hull Interaction and Determination of the Effective Wake Field Using a Hybrid RANS-BEM Approach," in *3rd International Symposium on Marine Propulsors*, Launceston, Australia, 2013.

[14] B. Aupoix, "Roughness Corrections for the k-ω Shear Stress Transport Model: Status and Proposals," *Journal of Fluids Engineering,* vol. 137, no. 2, 2014.

[15] L. Eça, M. Kerkvliet and S. L. Toxopeus, "On the Simulation of Turbulent Flows over Rough Walls Using the RANS Equations," in *24th Numerical Towing Tank Symposium (NuTTS)*, Zagreb, Croatia, 2022.